Clim Dyn (2011) 37:1601–1620
DOI 10.1007/s00382-010-0935-7

An assessment of the surface climate in the NCEP climate forecast system reanalysis

Wanqiu Wang · Pingping Xie · Soo-Hyun Yoo · Yan Xue · Arun Kumar · Xingren Wu

Received: 10 June 2010 / Accepted: 14 October 2010 / Published online: 28 October 2010

Abstract This paper analyzes surface climate variability in the climate forecast system reanalysis (CFSR) recently completed at the National Centers for Environmental Prediction (NCEP). The CFSR represents a new generation of reanalysis effort with first guess from a coupled atmosphere–ocean–sea ice–land forecast system. This study focuses on the analysis of climate variability for a set of surface variables including precipitation, surface air 2-m temperature (T2m), and surface heat fluxes. None of these quantities are assimilated directly and thus an assessment of their variability provides an independent measure of the accuracy. The CFSR is compared with observational estimates and three previous reanalyses (the NCEP/NCAR reanalysis or R1, the NCEP/DOE reanalysis or R2, and the ERA40 produced by the European Centre for Medium-Range Weather Forecasts). The CFSR has improved time-mean precipitation distribution over various regions compared to the three previous reanalyses, leading to a better representation of freshwater flux (evaporation minus precipitation). For interannual variability, the CFSR shows improved precipitation correlation with observations over the Indian Ocean, Maritime Continent, and western Pacific. The T2m of the CFSR is superior to R1 and R2 with more realistic interannual variability and long-term trend. On the other hand, the CFSR overestimates downward solar radiation flux over the tropical Western Hemisphere warm pool, consistent with a negative cloudiness bias and a positive sea surface temperature bias. Meanwhile, the evaporative latent heat flux in CFSR appears to be larger than other observational estimates over most of the globe. A few deficiencies in the long-term variations are identified in the CFSR. Firstly, dramatic changes are found around 1998–2001 in the global average of a number of variables, possibly related to the changes in the assimilated satellite observations. Secondly, the use of multiple streams for the CFSR induces spurious jumps in soil moisture between adjacent streams. Thirdly, there is an inconsistency in long-term sea ice extent variations over the Arctic regions between the CFSR and other observations with the CFSR showing smaller sea ice extent before 1997 and larger extent starting in 1997. These deficiencies may have impacts on the application of the CFSR for climate diagnoses and predictions. Relationships between surface heat fluxes and SST tendency and between SST and precipitation are analyzed and compared with observational estimates and other reanalyses. Global mean fields of surface heat and water fluxes together with radiation fluxes at the top of the atmosphere are documented and presented over the entire globe, and for the ocean and land separately.

Keywords Climate forecast system reanalysis · Atmospheric reanalysis · Surface climate variability · Long-term trend

W. Wang (✉) · P. Xie · S.-H. Yoo · Y. Xue · A. Kumar
Climate Prediction Center, NCEP/NWS/NOAA,
5200 Auth Road, Room 605, Camp Springs,
MD 20746, USA
e-mail: wanqiu.wang@noaa.gov

X. Wu
Environmental Modeling Center, NCEP/NWS/NOAA,
Camp Springs, MD, USA

1 Introduction

Since the development of the first generation of reanalysis systems (Schubert et al. 1995; Kalnay et al. 1996; Gibson et al. 1997; Kistler et al. 2001), global atmospheric reanalyses have become indispensable for climate research and

applications. Reanalysis products have been used in climate diagnostics, initialization and verification of climate prediction models, downscaling with statistical or regional dynamical models, and forcing oceanic models as surface boundary condition for simulations and assimilations. As the reanalyses have become the de facto tool for understanding climate variability and trends, validating them against independent observations is also a necessary task to assess their quality. Evaluations of the previous reanalyses have been conducted through intercomparisons among reanalyses, and comparisons against independent observations, to estimate their accuracy and to quantify uncertainties (e.g., Moore and Renfrew 2002; Wu et al. 2005; Cronin et al. 2006; Yu et al. 2006; Trenberth et al. 2007).

A climate forecast system reanalysis (CFSR) has recently been developed at the National Centers for Environmental Prediction (NCEP) (Saha et al. 2010). New features in the CFSR include: (1) it is the first reanalysis system in which the guess fields are taken as the 6-h forecast from a coupled atmosphere–ocean climate system with an interactive sea ice component; (2) it uses a higher horizontal resolution ($\sim$38 km) for the atmosphere than the previous atmospheric reanalyses; and (3) it assimilates satellite radiances rather than the retrieved temperature and humidity values. In addition, the CFSR is forced with observed estimates of evolving green house gas (GHG) concentrations, aerosols, and solar variations. The CFSR also assimilates hydrological quantities from a parallel land surface model forced by the NOAA's Climate Prediction Center (CPC) pentad merged analysis of precipitation (Xie and Arkin 1997) and the CPC unified daily gauge analysis (Xie et al. 2010).

In this study, we analyze surface climate and its variability in the CFSR. The primary focus is on precipitation, surface air 2-m temperature (T2m), soil moisture, sea surface temperature (SST), and the associated fields including surface heat and water fluxes, and precipitable water. Other aspects of the CFSR are examined in accompanying papers, including assessments of the oceanic (Xue et al. 2010), troposphere (Chelliah et al. 2010), and stratosphere (Long et al. 2010) variability. Most of the variables analyzed in this study are derived within the CFSR without an explicit assimilation of corresponding observations (for example, precipitation), and thus their assessment provides a plausible determination of the accuracy of the assimilated quantities in the CFSR. The scope of this analysis is outlined below.

1.1 How does CFSR compare with previous analyses and other observations for its rendition of climatology and variability?

The reanalyses have been widely used in climate studies. However, as the reanalysis assimilation systems are based on models that have various biases, inevitably there are errors in the reanalyses that must be considered in their application. For example, Onogi et al. (2007) found that precipitation rate in reanalyses was substantially larger than observational estimates, and there was an upward trend in the 1990s. Roads (2003) analyzed the atmospheric hydrologic cycle in the NCEP/NCAR reanalysis (R1, Kalnay et al. 1996), and NCEP/DOE reanalysis (R2, Kanamitsu et al. 2002), and found that both R1 and R2 produced excessive precipitation and evaporation compared with estimates derived from the tropical rainfall measuring mission (TRMM, Simpson et al. 1988).

Many studies have also indicated large uncertainties in surface heat fluxes in reanalyses, as well as in observational estimates, with the amplitude of global mean (GM) differences over oceans as large as more than 10 Wm^{-2} in latent heat flux and shortwave radiation. It is not atypical that the amplitude of the imbalance of net surface heat flux exceeds 20 Wm^{-2} (Smith et al. 2001; Kistler et al. 2001; Yu et al. 2007; Trenberth et al. 2009). However, as the reanalysis systems are moving towards the analysis of the Earth System as a whole, and the CFSR as a coupled atmosphere–ocean assimilation system is one such step in that direction, the accuracy of surface heat fluxes is critical for a correct representation of oceanic surface heat budget, a key variable for detecting climate trend resulting from radiative imbalance due to the anthropogenic activity.

Towards a validation of the CFSR's rendition of surface climate variability, we diagnose the climatology and variability of various surface variables. A comparison with previous NCEP reanalyses is made to assess the improvements with the CFSR.

1.2 Does the CFSR capture the observed long-term changes?

Observations have shown that the climate has undergone changes on multidecadal time-scales associated with changes in the external radiative forcing due to increasing GHG concentrations and volcanic eruptions together with variations that are internal to the climate system. In addition to the low-frequency climate variations that are physical, reanalyses may also contain spurious trends or discontinuities due to changes in input observational data. For examples, the lack of the effects of volcanic aerosols on HIRS infrared radiances following the eruption of Mt Pinatubo in ERA40 resulted in unrealistic large rainfall rates from the second half of 1991 onwards (Uppala et al. 2005), while the enhanced precipitation in the Japanese 25-year reanalysis (JRA25) after 1998 were argued to be related to changes in the input data from TIROS operational vertical sounder (TOVS) to ATOVS (advanced TOVS) in November 1998 (Onogi et al. 2007). Another

possible impact is the setup of the system to complete the reanalysis for the historical period. The CFSR used six separate parallel streams for different periods (Saha et al. 2010). Different streams were allowed to overlap for a year or so, and for each stream, reanalysis data during the spin-up period were discarded. Such a configuration may introduce a discontinuity from one stream to another when the time series from the final data is analyzed.

Long-term variations in reanalyses are important for climate prediction when they are used to initialize climate models. Cai et al. (2009) analyzed seasonal climate retrospective forecasts (or hindcasts) from the NCEP climate forecast system (CFS) in the context of warming trends due to GHGs and their influence on seasonal forecasts, and how the initial condition information about the trend evolves with the forecast lead-time. Wang et al. (2010) found a systematic cold bias over northern hemisphere mid-latitudes in the CFS forecasts for boreal warm seasons starting 2005. This cold bias was related to the soil moisture anomalies in the initial conditions from the R2 which were too wet.

Given the importance of climate trends, an analysis of long-term variations in the CFSR is also a focus of this study. We assess to what extent the reanalysis captures the observed trends, and how the trends may have been affected by the changes in the input data and by the switch between analysis streams.

1.3 How consistent are the relationships between atmospheric and oceanic fields in the CFSR with those in other reanalyses and observational estimates?

In a coupled atmosphere–ocean system, the atmosphere and ocean interact with each other through the exchange of surface energy, momentum, and water mass. However, the influence of air-sea interaction on the ocean and atmospheric evolution presents different characteristics at different locations. The atmospheric variability in the central-eastern tropical Pacific is primarily driven by the ocean surface conditions while the atmospheric variability over the other ocean basins acts to drive the local oceanic variability (Kumar and Hoerling 1998; Alexander et al. 2002; Wang et al. 2003; Shinoda et al. 2004; Wu and Kirtman 2005; Krishna Kumar et al. 2005). An implication is that the relationship between surface heat fluxes and SSTs, and between SSTs and the atmospheric response to SSTs, such as precipitation, can be different over different ocean basins. In regions where the interaction is dominated by the response in SSTs to atmospheric thermodynamic forcing (i.e., atmosphere driving the ocean), one would expect a positive relationship between surface net heat flux anomaly and SST anomaly tendency, while in regions where the atmospheric variability is controlled by the ocean, one would expect an atmospheric response to local SST anomalies.

The CFSR was developed to represent the observed coupled atmosphere–ocean system, and differed from the earlier reanalyses in that the first guess fields were from a 6-h coupled forecast, and not from an integration of an atmosphere-only model forced by the SST. Given the coupled versus uncoupled natures of guess fields during the assimilation cycle, it is anticipated that the variability at the ocean–atmosphere interface in the CFSR will be a better rendition of the observed variability. In the present analysis, the relationship between the net surface heat flux and SST tendency and that between SST and precipitation rate are analyzed for reanalysis data as well as observational data. As the observational surface heat fluxes over ocean are estimates derived from other variables from either in situ data only or from consolidated in situ and model data (e.g., Yu and Weller 2007; Berry and Kent 2009), and the observed precipitation over oceans are also estimates dominated by satellite-based retrievals (Xie and Arkin 1997; Adler et al. 2003), the focus of our analysis is on the consistency among reanalyses and observational estimates rather than the absolute errors in a particular reanalysis or observational estimate.

While it is important to highlight improvements in the new reanalysis compared to previous ones, we also identify deficiencies in the CFSR. Such a documentation helps provide a background for the user community in the application of the CFSR for climate studies. The analysis might be also useful in future reanalysis efforts for continued improvements,

The paper is organized as follows: Sect. 2 describes the data from the CFSR, and other reanalyses and observations; Sect. 3 documents the precipitation and E − P (evaporation minus precipitation) climatology, and SST bias and associated fields; Sect. 4 analyzes interannual variability of precipitation and T2m; Sect. 5 discusses long-term variations of global and regional means; Sect. 6 analyzes air–sea interaction; and Sect. 7 provides a summary.

2 Data

This analysis of the CFSR climatology and interannual variability is based on monthly-mean fields. The data span the period January 1979 to December 2008. A set of variables from the CFSR is analyzed, including precipitation, T2m, evaporation, surface latent heat flux (LH), surface sensible heat flux (SH), surface net downward solar radiation (SWsfc), precipitable water (PWAT), total cloud amount (CLD), SST, volumetric soil moisture (SM), and

sea ice concentration (SIC). Instantaneous SSTs at the beginning and the end of each month are used to compute monthly SST tendency. In addition, for one special case, 6-h precipitation for 0–6Z of July 1, 2007 is used to show the capability of the CFSR to capture individual weather systems that affect the variability at longer time scales.

Three previous reanalyses are used for comparison purposes: the European Centre for Medium-Range Weather Forecasts (ECMWF) ERA40 from 1979 to 2001, and the NCEP R1 and R2 from 1979 to 2008. Various observational analyses used for the assessment of the CFSR include:

Precipitation: The CPC merged analysis of precipitation (CMAP, Xie and Arkin 1997); the Global Precipitation Climatology Project (GPCP, Adler et al. 2003); and the CPC MORPHing technique (CMORPH, Joyce et al. 2004)

E − P: Mean climatology of observed E − P used in this study is defined based on mean values from a set of widely used products for a 13-year period from 1988 to 2000. The mean climatology of precipitation is an average of those for the GPCP, CMAP, and TRMM analyses. The climatology of oceanic evaporation, meanwhile, is from five data sets including the Goddard Satellite-based Surface Turbulent Flux Version 2 (GSSTF2) of Chou et al. (2003), the Hamburg Ocean Atmosphere Parameters from Satellite Data Version 3 (HOAPS3) of Grassl et al. (2000), the Japanese Ocean Flux with Use of Remote Sensing Observation Version 2 (J-OFURO2) of Tomita et al. (2010), the objective air–sea flux analysis (OAFlux) of Yu and Weller. (2007), and the COADS-based Southapmton Oceangraphy Centre (SOC) climatology of Josey et al. (1998, 1999). Combined use of multiple products reduces the quantitative uncertainties inherent in the individual data sets

SST: The National Climate Data Center (NCDC) optimum interpolation daily sea surface temperature analysis (OISST, Reynolds et al. 2007)

T2m: The CPC analysis based upon station data from both the Global Historical Climatology Network version 2 and the Climate Anomaly Monitoring System (GHCNCAMS, Fan and van den Dool 2008)

LH, SH: Analyzed air–sea heat fluxes (OAFlux, Yu and Weller 2007); and National Oceanography Centre Southampton flux dataset version 2 (NOCSv2, Berry and Kent 2009)

SWsfc: International Satellite Cloud Climatology Project (ISCCP) global radiative flux data (IDCCPFD, Zhang et al. 2004); NASA World Climate Research Programme/Global Energy and Water-Cycle Experiment (WCRP/GEWEX) Surface Radiation Budget (SRB) Project version 2.5; and NOCSv2

CLD: ISCCP; NOCSv2

Sea ice: National Snow and Ice Data Center (NSIDC)

3 Climatology

In this section, we present an analysis of the annual mean climatology. We will first compare spatial maps among reanalyses and observations for precipitation, SST and the related surface heat fluxes. Climatology of the full T2m field is not discussed in this section, as it strongly depends on the topography used for each reanalysis. GM fluxes at the surface and at the top of the atmosphere (TOA), and surface precipitation and evaporation will also be documented at the end of this section. Complementary analysis of surface turbulent fluxes of heat and momentum over oceans can be found in Xue et al. (2010).

3.1 Precipitation and E − P

Figure 1 shows annual mean precipitation climatology (contour) and differences (shading) between the observation and reanalyses. The observation is taken as the average of CMAP and GPCP. The climatology is defined as the 1979–2008 average, except for ERA40 for which the climatology is the average of 1979–2001. GM precipitation is given above each panel. Similar patterns are seen in the observation and reanalyses, with relatively large precipitation rates over the Intertropical Convergence Zone (ITCZ), the South Pacific Convergence Zone (SPCZ), and regions of the western ocean basins that are related to storm track activity, and relatively small precipitation rates in the eastern tropical ocean basins. The R2 and ERA40 are too wet over most of the tropics while the R1 is too dry over the ITCZ, SPCZ, and the equatorial eastern Indian Ocean and western Pacific. One common feature in the R1, R2, and ERA40 is a double-ITCZ structure in the tropical Pacific with smaller precipitation rate over the observed

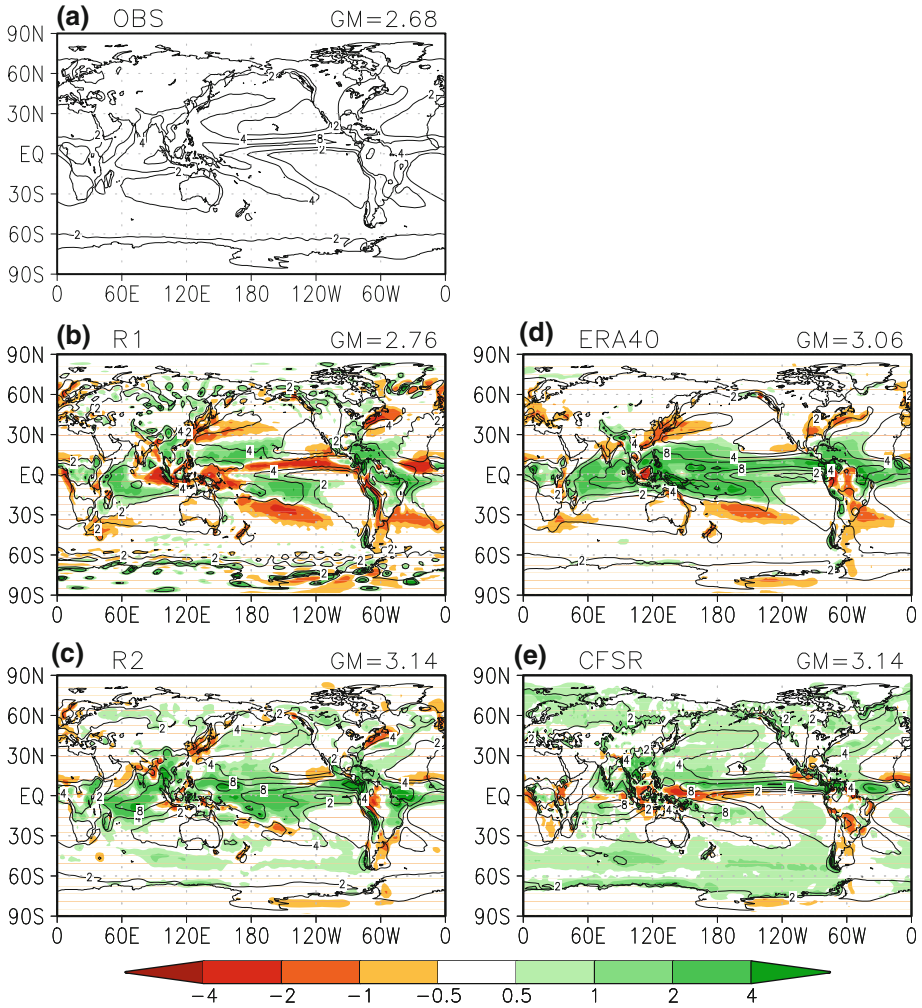

Fig. 1 Precipitation climatology (*contour*) and differences (*shading*) from the observation taken as the average of CMAP and GPCP. **a** Observation, **b** R1, **c** R2, **d** ERA40, and **e** CFSR. *Contours* are plotted at 2, 4, 8, and 12 mm/day, and *shadings* are at −4, −2, −1, −0.5, 0.5, 1, 2, and 4 mm/day. Global mean (GM) climatology is shown above each *panel*

SPCZ region. Such a double-ITCZ structure is a common error in many contemporary general circulation models (Dai 2006). This shortcoming does not exist in the CFSR. In addition, the CFSR produces better precipitation distribution over the tropical northwestern Pacific, the SPCZ, South America, and southeastern Pacific. Major differences in the CFSR include a dry bias over the Maritime Continent and the western Pacific, and a wet bias in ITCZ in the tropical Pacific and Atlantic and in the mid-high latitudes. Globally averaged, all reanalyses produce a larger rate than the estimate from CMAP and GPCP.

The E − P is not only an integral parameter of the atmosphere–ocean hydrological cycle and heat budget, it is also a forcing component of the oceanic circulation (Huang et al. 2005). We show the 1988–2000 average of E − P from various reanalyses and observations in Fig. 2. All reanalyses agree well with the observations with more precipitation than evaporation over most of the tropical Indian Ocean, the Maritime Continent, the western Pacific, the ITCZ and SPCZ, and more evaporation than precipitation in other tropical and subtropical regions. Such a distribution in the tropics and subtropics is controlled more by precipitation which has larger magnitude and is spatially less uniform than evaporation (not shown). However, a closer examination indicates that the CFSR produces a better distribution than the other three reanalyses over the tropical central Pacific. The pattern correlation between the observed annual mean E − P and that of the R1, R2, ERA40, and CFSR is 0.829, 0.876, 0.866, and 0.935, respectively. The E − P in the R1, R2, and ERA40 in the central Pacific has a more zonal orientation, resulting from the double-ITCZ-like structure in precipitation. In addition, the near-zero E − P in the tropical northwest Pacific is well reproduced in the CFSR, while the other three reanalyses produce negative E − P in this area. Comparison in precipitation and evaporation shows that this error in the R1, R2, and ERA40 is due to the combined effects of insufficient precipitation (Fig. 1) and excessive evaporation (not shown) compared to the observations and the CFSR. All three reanalyses compare well with the observation in the northern extratropics.

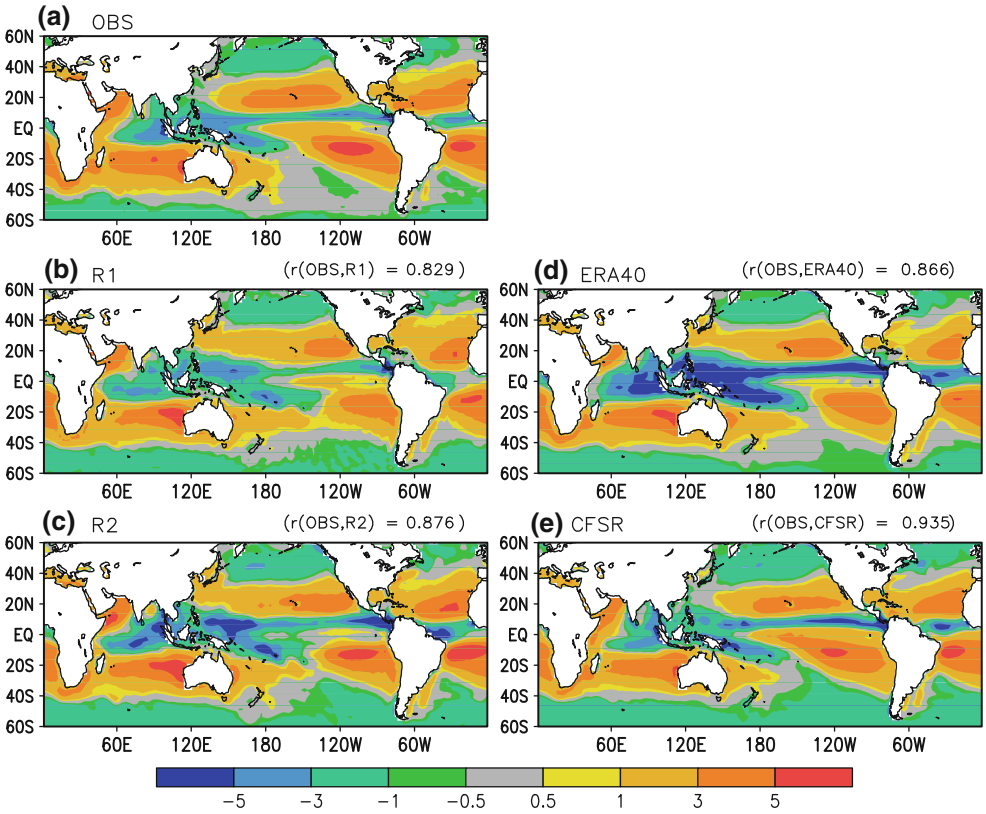

Fig. 2 1988–2000 average of E − P. **a** Observation, **b** R1, **c** R2, **d** ERA40, and **e** CFSR. Unit is mm/day and values are *shaded* at −5, −3, −1, −0.5, 0.5, 1, 3, and 5

3.2 SST, SWsfc and LH

Unlike the previous atmospheric reanalysis systems in which surface oceanic boundary conditions were prescribed, the SST in CFSR, taken as the temperature at the top level of 5-m depth, is allowed to evolve freely during the 6-h coupled model integration, which provides the first guess for the analysis (Saha et al. 2010). The annual mean differences between the first guess field (averaged over four assimilation cycles within each day) and NCDC daily OISST (Reynolds et al. 2007) for 1984–2004 are shown in Fig. 3a. These differences include the initial differences between the CFSR SST analysis and OISST, and the subsequent drift during the 6-h model integration.

The amplitude of the SST differences in the tropics is about 0.05–0.1 K. Positive SST errors present in the tropical Indian Ocean, the western Pacific, and tropical northern Atlantic. Negative errors are seen in the equatorial regions of the Atlantic and eastern Pacific. The positive SST errors in the tropical Indian Ocean, western-central Pacific, and northern Atlantic are possibly due to errors in SWsfc (Fig. 3b), which are defined as the departures of CFSR SWsfc from the average of three observational estimates: ISCCPFD (Zhang et al. 2004), WCRP/GEWEX SRB version 2.5, and NOCSv2 (Berry and Kent 2009). Compared to the observations, the CFSR produces excessive SW in the Tropics except in the southeastern Pacific and southern Atlantic (Fig. 3b). The SWsfc errors can be further related to the errors in total cloudiness defined as the differences between the CFSR and the average of ISCCP and NOCSv2 observations. Figure 3c shows that, relative to observational estimates, the CFSR produces too few clouds in the tropics except for the southeastern Pacific. Xue et al. (2010) showed that the CFSR has greatly corrected the deficiency of the net surface heat fluxes in the tropics in R1 and R2 due to the increased SWsfc. However, the SWsfc in CFSR appears to be too large over the Western Hemisphere warm pool because of the deficiency in cloudiness.

Differences in LH between the CFSR and observation (average of OAflux and NOCSv2) are also calculated to examine its impacts on SSTs (Fig. 3d). It is seen that the CFSR produces larger evaporative cooling than the observational estimates over almost the entire ocean surface. However, such a larger evaporative cooling in the CFSR cannot explain the overall warm SST bias in the CFSR (Fig. 3a), although the CFSR cold SST bias in the equatorial eastern Pacific may be related to the excessive evaporation. Errors in net downward surface longwave radiation and sensible heat flux are much smaller in

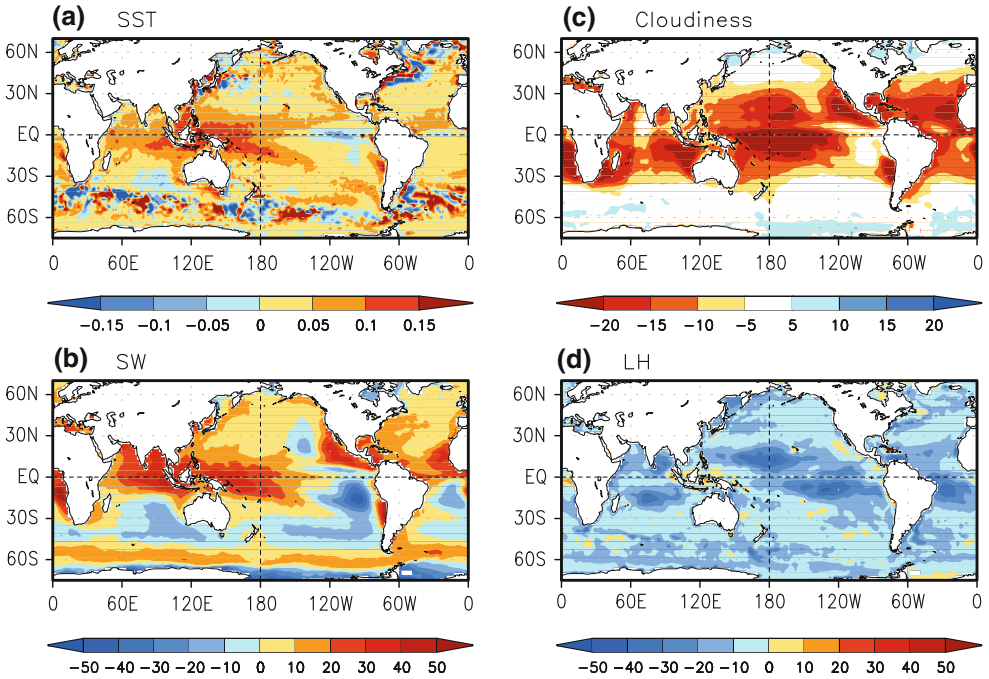

Fig. 3 1984–2004 annual mean differences between the CFSR and observations. **a** Sea surface temperature (SST), **b** surface downward solar radiation (SWsfc), **c** cloudiness (CLD), **d** surface latent heat flux (LH). The values are *shaded* at an interval of 0.05 K for SST, 10 Wm^{-2} for SW and LH, and 5% for CLD

amplitude compared to those in SWsfc and LH (not shown). These results suggest that the CFSR SST errors are related to errors in SWsfc that are due to reduced cloudiness in the reanalysis, with some potential impacts from evaporative cooling that is too strong in the eastern Pacific and Atlantic.

Since the CFSR SST is nudged to the OISST at the beginning of each cycle (Saha et al. 2010), the differences between the 6-h CFSR forecasts and the OISST in Fig. 3a represent the accumulative impacts of the different processes during the 6-h integration. If the SST differences are all attributed to errors in surface net heat flux that is used to warm up the top level (10 m) of the ocean, a total of 200 Wm^{-2} would be needed. This suggests that the SST errors in Fig. 3a cannot be explained by the errors in the net surface heat flux alone. Other contributing factors include the errors in dynamic forcing (momentum fluxes), deficiencies in oceanic dynamics, and the uncertainties in the OISST.

3.3 Global mean heat and water fluxes

Observational estimates of GM heat and water fluxes have been made in various studies, and comparisons with reanalyses reveal large differences (Yu et al. 2008; Berry and Kent 2009; Trenberth et al. 2009). Following past approaches, in this subsection we document global heat and water flux components at the surface in the CFSR and their comparison with the R1 and R2. GM heat fluxes are given in Table 1. Net radiation fluxes at the top of the atmosphere and the planetary albedo are also included.

The CFSR produces larger SWsfc over the ocean than the R1 and R2 (Table 1), resulting in a larger GM SWsfc, although the CFSR SWsfc over land (140.4 Wm^{-2}) is smaller than that in the R1 (152.7 Wm^{-2}) and R2 (142.6 Wm^{-2}). The larger SWsfc over the ocean in the CFSR is likely due to the reduced cloudiness in the tropics compared to the R1 and R2 (not shown). Differences in the net downward longwave radiation flux at the surface (LWsfc) between the CFSR and the two previous NCEP reanalyses (R1 and R2) are smaller than those in SWsfc. The CFSR generates smaller LH but larger SH over land than the R1 and R2. Over the ocean, LH (SH) from the CFSR is larger (smaller) than that from R1 but smaller (larger) than that from R2. Since both R1 and R2 have been shown to produce larger LH compared with observational estimates (Yu et al. 2008), the CFSR LH is probably also too large as suggested by Fig. 3d. Net downward heat flux (NETsfc) in all reanalyses is positive over the globe, with the CFSR producing the larger positive imbalance (9.7 Wm^{-2}) than the R1 (3.5 Wm^{-2}) and R2 (4.8 Wm^{-2}). Over the ocean, the net imbalance is 13 Wm^{-2} in the CFSR, compared to the imbalance of 3.7 and 4.1 Wm^{-2} in the R1 and R2. These results indicate that substantial errors remain in the surface heat fluxes in the new generation CFSR, and are similar to observational estimates which

Table 1 1979–2008 90S–90N average surface downward solar radiation (SWsfc), surface sownward longwave radiation (LWsfc), upward latent heat flux (LH), upward sensible heat flux (SH), net downward sufrace heat flux (NETsfc), outgoing longwave radiation (OLR), downward solar radiation at the TOA (SWtoa), net downward radiation at the TOA (NETtoa), planetary albedo (ALBtoa)

	Reanalysis	SWsfc	LWsfc	LH	SH	NETsfc	OLR	SWtoa	NETtao	ALBtoa
Global	R1	161.3	−60.9	81.4	15.5	3.5	237.4	225.7	−11.7	34.00
	R2	160.2	−56.8	90.9	7.7	4.8	243.2	236.0	−7.2	30.86
	CFSR	167.0	−57.2	83.8	16.3	9.7	243.5	244.0	0.5	28.58
Ocean	R1	164.7	−56.1	93.7	11.2	3.7	239.5	231.4	−8.1	33.5
	R2	167.2	−51.2	106.1	5.8	4.1	245.7	243.2	−2.5	29.9
	CFSR	177.9	−53.5	102.6	8.8	13.0	246.8	256.5	9.7	26.3
Land	R1	152.7	−73.1	50.6	26.4	2.6	232.1	211.4	−20.7	35.4
	R2	142.6	−70.9	52.4	12.5	6.8	237.0	217.9	−19.1	33.3
	CFSR	140.4	−66.1	37.6	34.7	3.0	235.4	213.4	−22.0	34.6

Unit of heat fluxes is Wm^{-2}. ALBtoa is shown as percentage

also show large imbalances in global surface heat fluxes (Berry and Kent 2009).

The GM balance of radiation fluxes at the TOA (NETtoa) in the CFSR is 0.5 Wm^{-2}, much better than the large imbalance in R1 (−11.7 Wm^{-2}) and R2 (−7.2 Wm^{-2}). The improved balance of radiation fluxes at the TOA is largely due to the increased net downward solar radiation (SWtoa) over the ocean (256.5 Wm^{-2} in CFSR compared to 231.4 Wm^{-2} in R1 and 243.2 Wm^{-2} in R2), corresponding to a much smaller planetary albedo in the CFSR (26.3%) compared to 33.5% in R1 and 29.9% in R2. One piece of additional information that can be inferred from Table 1 is the larger atmospheric absorption of solar radiation in the CFSR (77 Wm^{-2}) than those in R1 (64.6 Wm^{-2}) and R2 (75.8 Wm^{-2}). Since the cloudiness in the tropical oceans is smaller in the CFSR than that in R1 and R2 (not shown), the larger atmospheric absorption of solar radiation in the CFSR implies a wetter atmosphere, which is consistent with the results in Chelliah et al. (2010).

Precipitation (P), evaporation (E), and their differences (E − P) are shown in Table 2. The CFSR and R2 generate larger GM precipitation (3.14 mm/day) than the R1 (2.76 mm/day) due to more precipitation over the ocean. The GM precipitation rate in all three NCEP reanalyses is higher than the observational estimate (Fig. 1), consistent with results in previous studies (Roads 2003; Onogi et al. 2007). Over the land, the CFSR precipitation rate is about 0.1 mm/day higher than the R1 and R2. The GM evaporation rate is highest in the R2 and lowest in the R1 with the CFSR in between. GM E − P is close to 0 in the R1 and R2, implying that the evaporation rate is too high in all three reanalyses assuming that E − P is also near zero in nature and given that (1) the GM precipitation rate in the R1 and R2 is too high compared with observational estimates, and (2) evaporation in the CFSR is higher than that in the R1. The GM E − P in CFSR is −0.24 mm/day, suggesting that during the assimilation cycle the analysis system may inject additional moisture from atmospheric observations, which then gets precipitated out.

Table 2 1979–2008 90S–90N average surface precipitation (P), evaporation (E), and E − P (mm/day) from the R1, R2, and CFSR

	Reanalysis	P	E	E − P
Global	R1	2.76	2.82	0.06
	R2	3.14	3.14	0.00
	CFSR	3.14	2.90	−0.24
Ocean	R1	2.95	3.24	0.29
	R2	3.48	3.67	0.19
	CFSR	3.44	3.55	0.11
Land	R1	2.29	1.75	−0.54
	R2	2.28	1.81	−0.47
	CFSR	2.41	1.30	−1.11

4 Variability

In this section, we assess the variability of precipitation and T2m. We begin with a comparison of precipitation among R1, R2, and CFSR to see if changes in model physics during the past 15 years or so, together with the use of much higher resolution of the CFSR, lead to an improved representation of observed weather systems. We will then move on to a comparison of interannual variability of monthly anomalies among reanalyses and observations.

Precipitation rate during a 6-h period from 00Z to 06Z on 1 July 2007 is shown in Fig. 4. Both the CFSR and the earlier reanalyses (R1 and R2) capture most of the observed weather systems in the mid-latitudes in both hemispheres. However, the CFSR clearly reproduced a better spatial structure of the systems. For example, the

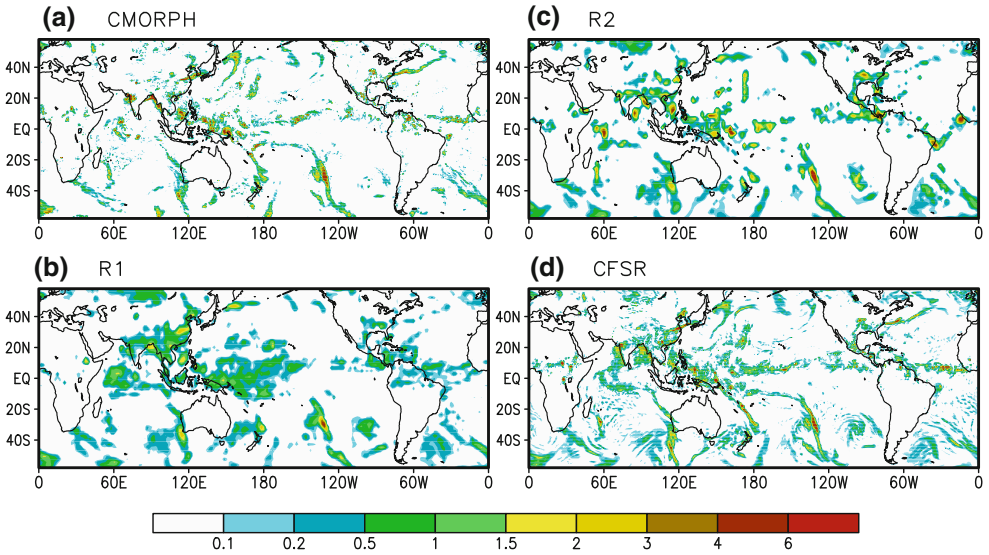

Fig. 4 Precipitation rate from 00Z to 06Z on 1 July 2007. **a** CMORPH, **b** R1, **b** R2, and **d** CFSR. Values are *shaded* at 0.1, 0.2, 0.5, 1, 1.5, 2, 3, 4, and 6 mm/h

system east of the Kuril Islands and south of the Kamchatka Peninsula in the northwest Pacific was not captured in the R1 and R2, but was well represented in the CFSR. In the Tropics, the CFSR appears to be much better in capturing the observed precipitation over the far western Pacific, ITCZ and SPCZ regions. Since variability at longer time scale results from accumulation of individual systems, the better performance of the CFSR in reproducing weather events may also lead to an improved representation of climate variability. The CFSR tends to cover wider raining areas. Part of this discrepancy may be attributable to the uncertainties in the CMORPH satellite estimates in capturing light precipitation over high latitudes (Ebert et al. 2007).

The spatial patterns of the interannual standard deviation of monthly mean precipitation for the observations (CMAP and GPCP) and reanalyses are shown in Fig. 5, and these patterns are similar to the climatological mean precipitation (Fig. 1). The patterns of the standard deviation for CMAP and GPCP are similar to each other although the GPCP indicates smaller amplitude over the eastern Indian Ocean, the Maritime Continent and western Pacific (Fig. 5a, b). In the tropical Pacific, the largest standard deviations in the R1, R2, and ERA40 are more zonally distributed (Fig. 5c, d, and e), consistent with the double-ITCZ-like structure in the climatology (Fig. 1c, d, and e), while the pattern in the CFSR (Fig. 5f) is more comparable to the observed estimates. The R1 amplitude is too weak over most of the tropical oceans while the variability in the R2 and ERA40 is much too strong. The CFSR variability in the tropics is also stronger than the observed but its amplitude is much reduced compared to that in the R2.

Another quantity we calculated to assess the performance of the reanalyses is the correlation with the observation. Spatial maps of temporal correlation of monthly mean precipitation between the CMAP and individual reanalyses are shown in Fig. 6. It is interesting to see that the R1 and R2 have higher correlation than the ERA40 and CFSR in the polar regions (poleward of 60°N and 60°S or so). However, within 60S to 60N, the correlation of the R1 and R2 is generally lower than the ERA40 and CFSR over both the land and ocean. The ERA40 shows better correlation in most of the northern mid-latitudes (30N–60N) and southern mid-latitudes (30S–50S) than the three NCEP reanalyses. *The most obvious improvement in the CFSR is in the Tropics where it has the highest correlation over almost the entire tropical belt*. In particular, the CFSR shows better performance over the Indian Ocean, the Maritime Continent, and western Pacific than the R1, R2 and ERA40.

For T2m over land, all reanalyses show a lower correlation in the tropical regions than in the mid-high latitudes (Fig. 7). The ERA40 is the best among the reanalyses examined in this study because observed T2m was combined in the post-processed ERA40 products (Uppala et al. 2005). Compared to the R1 and R2, the CFSR shows improved correlation over various regions including east China, western North America, and southern parts of Australia. Since observed T2m is not explicitly assimilated in all NCEP reanalyses, this improvement reflects the contribution of the upgraded representation of physical processes, and the use of time varying GHGs and aerosols.

Time series of the annual means of monthly spatial correlation with CMAP is shown in Fig. 8 to further

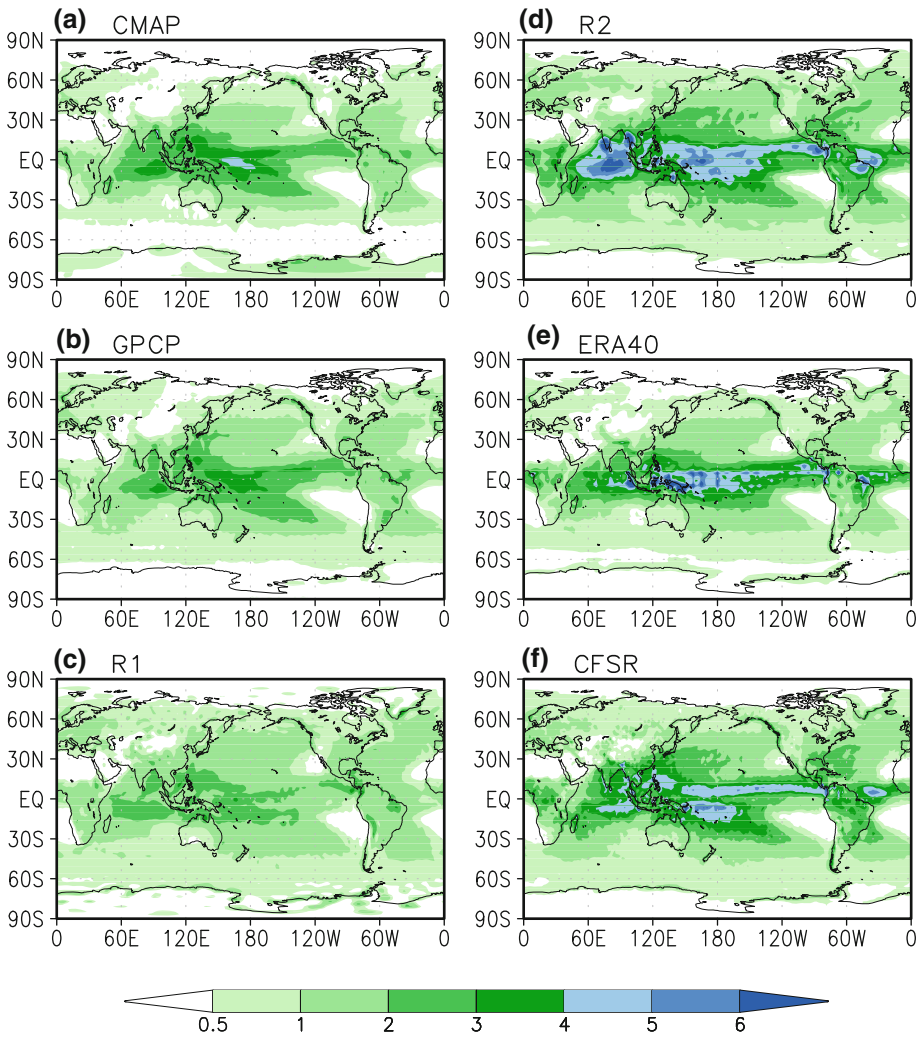

Fig. 5 Interannual standard deviation of monthly mean precipitation. **a** CMAP, **b** GPCP, **c** R1, **d** R2, **e** ERA40, and **f** CFSR. Values are *shaded* at 0.5, 1, 2, 3, 4, 5, and 6 mm/month

quantify the performance of the reanalyses. Correlation between the CMAP and GPCP is also plotted (black curve in Fig. 8) as a measure of uncertainty in the observations. It is seen that the CFSR shows the best performance throughout the period. Among the three previous reanalyses, R2 has the smallest correlation and ERA40 is overall the best. As shown in Fig. 6, the high global pattern correlation in the CFSR is mainly due to its better performance in the Tropics. In addition, the CFSR correlation is about 0.2 lower than the correlation between GPCP and CMAP, indicating that there may still be a large room for improvement in the next generation of reanalyses.

For T2m, the ERA40 shows the highest correlation among the reanalyses (Fig. 9), consistent with the spatial distributions of temporal correlation (Fig. 7). The CFSR is consistently better than the R1 and R2. It is interesting to see that the R1 and R2 have similar skill before 1999. Starting in year 2000, the R2 appear to generate better global T2m than the R1. We are not aware of the reason for this difference between these two previous NCEP reanalyses.

5 Long-term changes

Observed climate variations contain fluctuations on different time scales extending from seasonal to decadal and long-term trends. Analysis of the long-term trend is becoming increasingly important in the context of the possible influence from anthropogenic causes. In this section we analyze long-term fluctuations in GM quantities. The long-term changes considered here are the variability beyond interannual time scale. Because of the addition or removal of observational platforms as the assimilation progresses, a reanalysis product may also contain spurious trends or discontinuities that are not physical in nature and are an artifact of the assimilation system alone. In addition, a reanalysis with multiple streams like the CFSR may further introduce discontinuities between two adjacent streams even with a spin-up period across the overlapping streams.

The temporal evolution of annual average GM precipitation rate is shown in Fig. 10. Except for the R1 during the

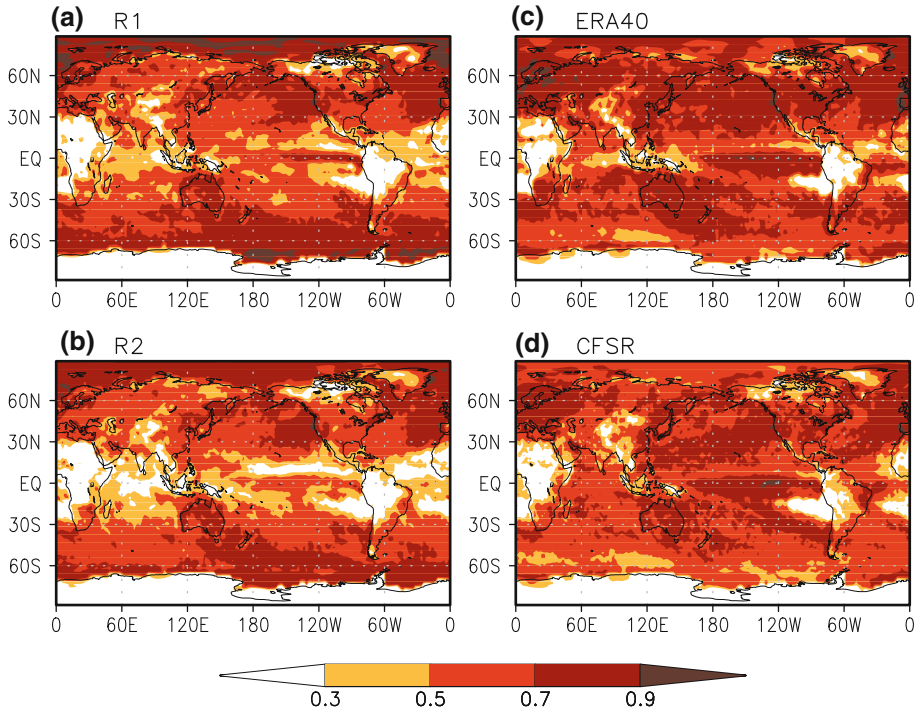

Fig. 6 Temporal correlation of monthly mean precipitation with the CMAP. **a** R1, **b** R2, **c** ERA40, and **d** CFSR. Values are *shaded* at an interval of 0.2 starting from 0.3

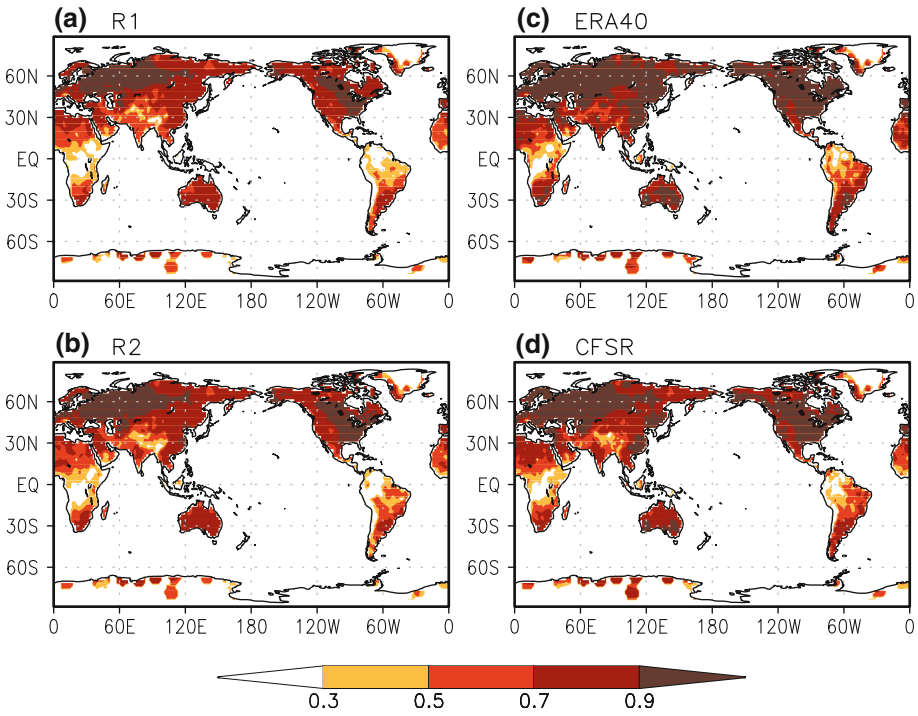

Fig. 7 As in Fig. 6 but for T2m correlation with GHCNCAMS

first several years (1979–1986), all reanalyses produced larger annual mean precipitation than the CMAP and GPCP estimates. There exist systematic differences among the reanalyses with the R1 producing the smallest time-mean precipitation rate. The R1, R2, and GPCP show increasing trends during the 1990–1997/1998 period, whereas CFSR continues increasing until about 2006. The ERA40 shows substantial interannual fluctuations with a large trend which was attributed to the unrealistic representation of aerosol influence from Mt Pinatubo (Uppala et al. 2005).

The temporal evolution of annual averages of GM T2m anomalies from GHCNCAMS and NCEP reanalyses is shown in Fig. 11. These reanalyses produced similar

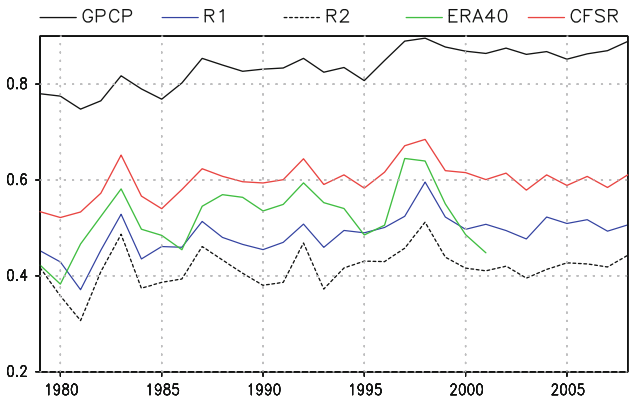

Fig. 8 Annual mean of spatial correlation with the CMAP of global precipitation for GPCP (*black*), R1 (*solid blue*), R2 (*dashed black*), ERA40 (*green*), and CFSR (*red*)

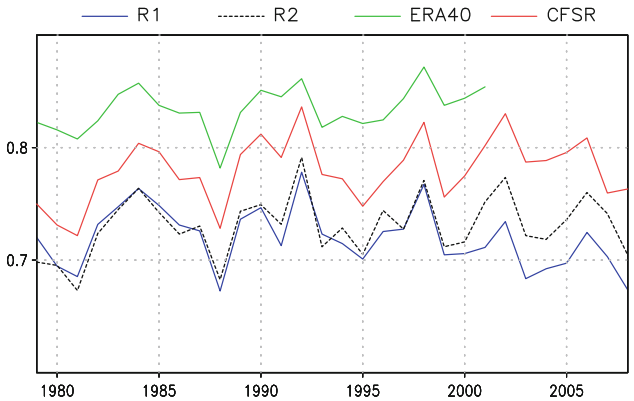

Fig. 9 Annual mean of spatial correlation with the GHCNCAMS of global land surface T2m for R1 (*solid blue*), R2 (*dashed black*), ERA40 (*green*), and CFSR (*red*)

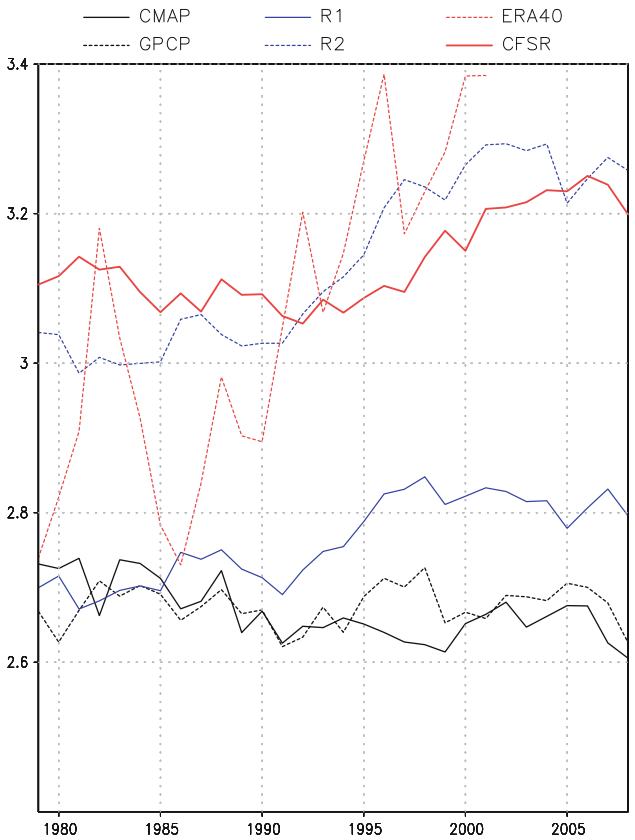

Fig. 10 Annual mean of global average precipitation (mm/day) for CMAP (*solid black*), GPCP (*dashed black*), R1 (*solid blue*), R2 (*dashed blue*), ERA40 (*dashed red*), and CFSR (*solid red*)

temporal fluctuations to those in the observations with an overall long-term warming trend. The CFSR showed a better performance than the R1 and R2 in reproducing both interannual variability and long-term trend. Anomalies in CFSR are generally closer to the observed than those in the R1 and R2. In particular, anomalies from the R1 and R2 were warmer before 1990 but cooler after 1999 than those in the CFSR, resulting in a smaller trend in the R1 (0.19 K/decade) and R2 (0.24 K/decade) than in the CFSR (0.35 K/decade) which is same as in the observed (Table 3). This may be a consequence of the fact that both R1 and R2 utilized a fixed value of CO_2, while that was not the case for the CFSR (Cai et al. 2009).

Annual mean time series of SWsfc, LWsfc, CLD, PWAT, surface evaporation, and precipitation averaged over the ocean, land and the globe from the CFSR are shown in Fig. 12 to analyze long-term changes in the CFSR, if any. All plotted global average quantities showed a significant change in 1998, primarily due to the change in the average over the ocean. GM surface evaporation decreased from 1998 to 1999 (Fig. 12e). GM CLD, precipitation, and PWAT showed an increase starting 1998 till 2001 (Fig. 12c, d and f). GM SWsfc (LWsfc) decreased (increased) from 1998 to 2001 (Fig. 12a, b), consistent with the increase in cloudiness (Fig. 12c). The decrease in SWsfc and the increase in CLD continued through 2007.

It is difficult to validate these long-term trends against observations which may contain large uncertainties. For example, Dai et al. (2006) showed that even the sign of cloud-cover trends in the tropics was different between surface observations and satellite data. Here we examine possible impacts due to the input observational data. The changes during 1998–2001 may have been related to the changes in the assimilated observational data. To illustrate this, GM monthly PWAT increment averaged over all 6-h cycles is shown in Fig. 13 together with global monthly mean P − E for comparison. The PWAT increment is the total amount of water added to the guess field of the 6-h forecast in the assimilation system to produce the best estimate of the state of the nature. There are two instances of significant increase in the PWAT increment, one in 1998 and the other in 2001. The significant increase in 1998 is

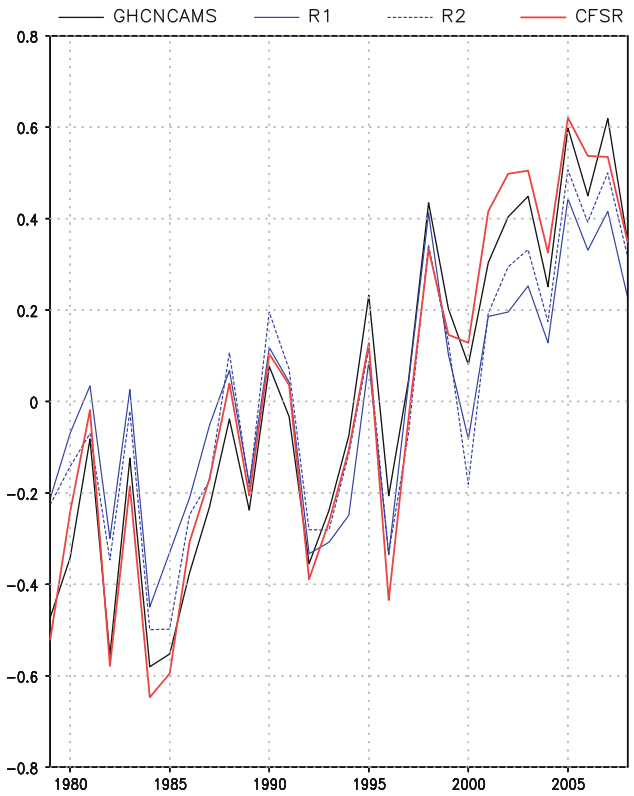

Fig. 11 Annual mean of global average of land surface T2m anomalies (K) for GHCNCAMS (*solid black*), GPCP R1 (*solid blue*), R2 (*dashed blue*), and CFSR (*solid red*)

Table 3 Global mean land surface T2m linear trend in the GHCNCAMS observation, R1, R2, and CFSR (K/decade)

Obs/reanalysis	GHCNCAMS	R1	R2	CFSR
Trend (K/decade)	0.35	0.19	0.24	0.35

likely due to the change from TOVS to ATOVS which resulted in dramatically more observed data in the assimilation system (Saha et al. 2010). The cause for the increase in PWAT increment in 2001 is less clear. One probable cause is the assimilation of QuikSCAT sea winds (Saha et al. 2010). Significant changes during 1998–2001 in the CFSR were also found in oceanic fields (Xue et al. 2010).

Another factor that could affect the long-term variations in the CFSR is the use of multiple streams for the reanalysis, which may induce discontinuity in the temporal evolution. Such a discontinuity indeed exists in certain fields that have long adjustment time-scale such as temperatures in the stratosphere (Long et al. 2010) and oceanic subsurface (Xue et al. 2010). Another variable that may also suffer from the merging across streams is soil moisture for which a spin-up of one-year or so may be too short. Figure 14 shows total volumetric soil moisture averaged for the tropics (30S–30N), southern hemisphere (60S–30S), and northern hemisphere (30N–70N). The vertical lines in Fig. 14 indicate the beginning of each stream after the spin-up period. It is seen that there exist trends in all three regions within the streams. For example, there is a downward trend starting January 1979, January 1990, and April 1999 in the tropics, a downward trend starting January 1979 and April 1999 in the southern hemisphere, and an upward trend in streams before April 2005 in the northern hemisphere. These varying trends within individual streams make it difficult to analyze the real signal of variability in soil moisture with the CFSR data. Differences of the same calendar month among different years due to these trends may also impact climate predictions initialized from the CFSR. Further analyses are needed to examine the geographical distribution of the trends.

One of the new features of the CFSR is that the first guess is from a coupled model that includes the prediction of sea ice concentration and thickness. Recent studies have shown that sea ice is a critical component in the climate system and for climatic variability (Francis et al. 2009; Serreze et al. 2009). The large downward trend in the Arctic sea ice in recent years and its causes have been a focus in various studies. An accurate representation of sea ice in the CFSR is important for its use in climate diagnoses as well as initialization of climate prediction. A comparison of sea ice coverage in the Northern Hemisphere between NSIDC and CFSR for September when the Arctic sea ice is at its seasonal minimum is presented in Fig. 15.

The CFSR reanalysis used sea ice data from Goddard Space Flight Center (GSFC) and NCEP (Saha et al. 2010). Before 1997, the CFSR sea ice reanalysis largely rely on the GSFC analysis. Starting in 1997, both GSFC and the NCEP sea ice analyses were used in the CFSR. The sea ice extent (Fig. 15a), defined as the sum of areas (including the open water area within the pack ice) where sea ice concentration is greater than 15%, from both NSIDC and CFSR shows similar interannual fluctuations with an overall decreasing trend with a record minimum in 2007. The sea ice extent in CFSR is slightly smaller before 1997 but larger starting 1997 than that in NSIDC. One factor that may result in differences between the NSIDC and CFSR is the use of different grids in the two data sets. However, this does not explain the change of the relative differences between the NSIDC and CFSR before and after 1997, as it would induce a consistent difference in sea ice extent between the two data sets. The smaller extent in the CFSR before 1997 is due to additional quality control on top of the GSFC data to filter out erroneous ice while the larger extent after 1997 is likely related to the addition of more points to include large lakes like Lake Ladoga and Lake Onega, as well as the Caspian Sea (Grumbine 2009, 2010a, b). Figure 15 also compares spatial sea ice coverage for 1998

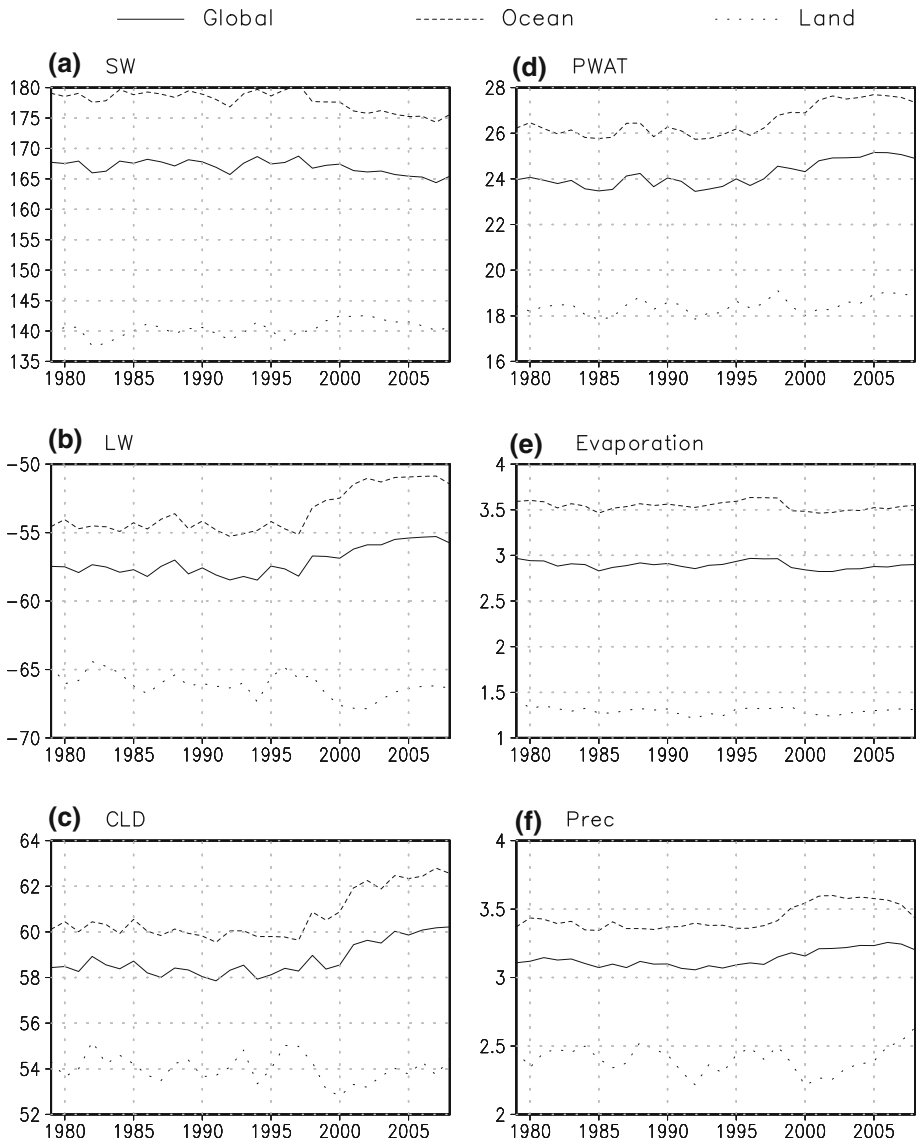

Fig. 12 Annual mean of global average of **a** surface downward solar radiation (SW, Wm^{-2}), **b** surface downward longwave radiation (LW, Wm^{-2}), **c** total cloud amount (CLD, %), **d** atmospheric precipitable water (PWAT), **e** evaporation (mm/day), and **f** precipitation (mm/day). Averages over the ocean, land, and the globe are plotted with *short-dashed curves*, *dotted curves*, and *solid curves*

when sea ice extent was at its maximum and 2007 when sea ice was at the record low. It is seen that the spatial distribution of sea ice and its contrast between the 2 years are very similar between NSIDC and CFSR.

6 Air-sea interaction and coupling

In this section, we compare the relationship between SST tendency and surface heat flux among reanalyses and observations. This analysis helps address the question that to what extent the SSTs are forced by local atmospheric heat fluxes. In addition we analyze the relationship between SST and precipitation to examine the response of precipitation to SST forcing.

Figure 16 shows the anomaly correlation between monthly SST tendency and monthly mean net heat flux. The monthly SST tendency is taken as the SST change from the beginning to the end of each month divided by the number of days of the month. A significance test has been applied to the anomaly correlation and only values that are at 95% significance level are plotted. The level of significance is estimated based on the Monte Carlo approach whereby correlations are computed after randomizing the heat flux. This procedure is repeated 10,000 times, and significance is estimated based on the percentage of times the actual correlation exceeds correlations achieved with the randomized set. Positive correlations in the NOCS which uses in situ observations only are mostly confined to the Northern Hemisphere with near zero values in the Southern Hemisphere where the in situ observations are quite sparse. The OAFlux and all reanalyses show a similar correlation distribution with relatively larger values (>0.3) in the subtropics and extratropics (poleward of 15S and

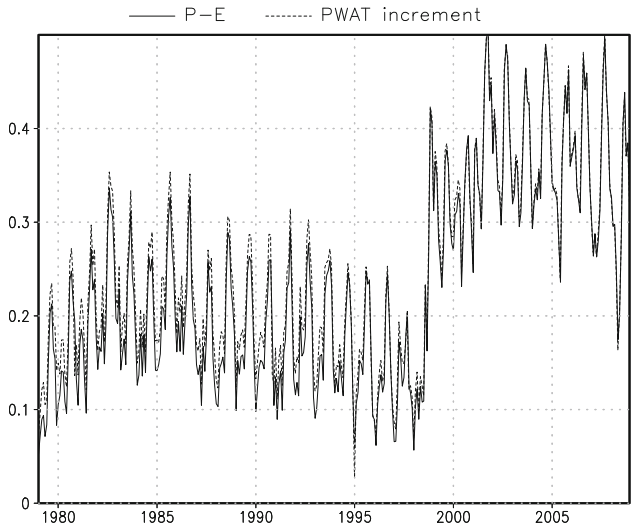

Fig. 13 Monthly mean of global average of PWAT increment (*solid*) and P − E (*short dashed*)

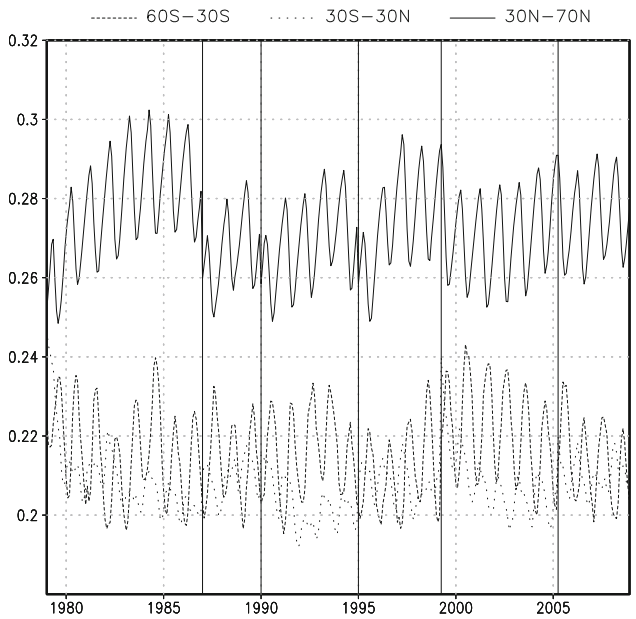

Fig. 14 Monthly mean of volumetric soil moisture for the average for the southern hemisphere (60S–30S, *short dashed*), northern hemisphere (30N–70N, *solid*), and tropics (30S-30N). *Vertical lines* indicate the beginning of each stream after the spin-up period

15N or so), demonstrating the impact of the heat flux on SSTs in these regions. In the tropical Pacific and Atlantic, the correlation is near zero in both observations and reanalyses, indicating that SST changes are dominated by oceanic dynamics. The correlation in the tropical Indian Ocean is also very small in the reanalyses although some positive correlations off the equator are seen in the OA-Flux. The similarity among the reanalyses indicate that the new features in the CFSR such as the higher resolution and the use of an atmosphere–ocean coupled model did not lead to any significant change in the SST-heat flux relationship, implying that when the SSTs were prescribed from observations (as in the R1, R2 and ERA40) or when they were very close to observations (as in the CFSR), the surface heat flux variability is largely determined by the assimilation of atmospheric fields.

Correlation between anomalous monthly mean precipitation and SST is presented in Fig. 17. As in Fig. 16, a significance test based on the Monte Carlo approach has been applied to the correlation and only values at 95% significance level are plotted. The distribution of the correlation based on observations shows a clear relationship between precipitation and SST anomalies across the tropical Pacific and Atlantic Oceans which can be inferred as a response of atmospheric general circulations to SST anomalies associated with El Nino/Southern Oscillation and Atlantic Nino. A weakly negative SST-precipitation relationship is found over most of the extratropics (Fig. 17a). All reanalyses captured the observed positive correlation in the tropical Pacific and Atlantic. In the subtropical Pacific and Atlantic, however, the R1, R2, and ERA40 produce too strong precipitation response, while the distribution in the CFSR is more realistic. In addition, the R1 and ERA40 show a weak positive correlation in the subtropical southern Indian Ocean (Fig. 17b, d), while the R2 and CFSR show little correlation (Fig. 17c, e), consistent with observations. The negative correlations in the mid-latitudes from the observations are not as clear in the renalyses. *Overall, the CFSR simulates the observed SST-precipitation relationship better than the other three previous reanalyses.*

7 Summary

A new reanalysis product, the CFSR, has been recently developed at the National Centers for Environmental Prediction (NCEP). The CFSR is the first climate reanalysis that includes both the atmosphere and ocean. This paper assesses the representation of surface climate and its variability in the CFSR. Aspects examined in this study include climatology, interannual variability, long-term changes, and the local relationship between atmospheric and oceanic fields. The CFSR is compared with observational estimates and three previous reanalyses NCEP/NCAR reanalysis (R1), NCEP/DOE reanalysis (R2), and ERA40.

The CFSR successfully reproduced the observed mean precipitation spatial pattern with improved precipitation distribution over the tropical northwestern Pacific, the SPCZ, South America, and southeastern Pacific compared to R1, R2 and ERA40. In particular, the double-ITCZ-like structure in the tropical Pacific in R1, R2 and ERA40 does not exist in the CFSR due primarily to the improved

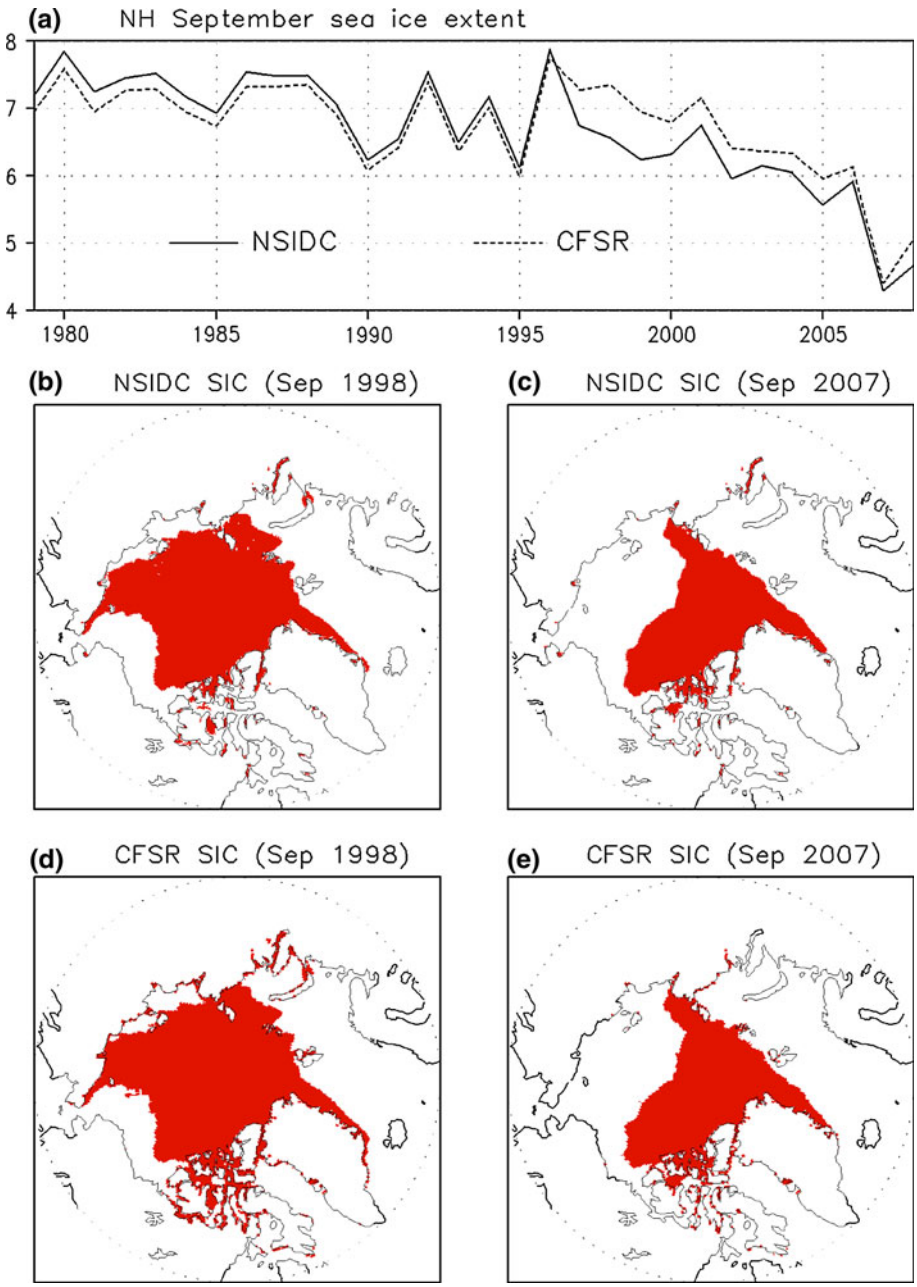

Fig. 15 **a** Time series of September Northern hemisphere sea ice extent (106 Km^2) from NSIDC (*solid*) and CFSR (*short dashed*); **b** September 1998 sea ice coverage in NSIDC; **c** September 1998 sea ice coverage in CFSR; **d** September 2007 sea ice coverage in NSIDC; and **e** September 2007 sea ice coverage in CFSR. Sea ice extent is defined as the sum of areas where sea ice concentration is >15%

precipitation over the SPCZ. The improved precipitation distribution in the CFSR also leads to a better representation of water flux (evaporation minus precipitation or E − P). Possible errors in the CFSR include a dry bias over the equatorial Indian Ocean, Maritime Continent, and western Pacific, and a wet bias in the mid-high latitudes.

The sea surface temperature is a prognostic variable in the CFSR and subject to errors in surface fluxes and dynamical processes. There are positive errors in the 6-h coupled forecast SST in most of the tropics. Negative errors exist in the equatorial Atlantic and eastern Pacific. The positive SST errors might be due to excessive surface downward solar radiation (SWsfc) in the CFSR. Upward surface latent heat flux in the CFSR is larger than observational estimates over most of the global ocean but does not explain the warm tropical SST errors in the CFSR.

GM of the 1979–2008 average of the heat balance at the surface and the top of the atmosphere and water fluxes at the surface is compared among the three NCEP reanalyses. SWsfc in the CFSR over the ocean (land) is larger (smaller) than that in the R1 and R2. The larger SWsfc over the ocean in the CFSR is related to smaller cloud amount which also results in larger downward solar radiation at the top of the atmosphere and smaller planetary albedo. All reanalyses produce too much precipitation, compared to observations. GM evaporation

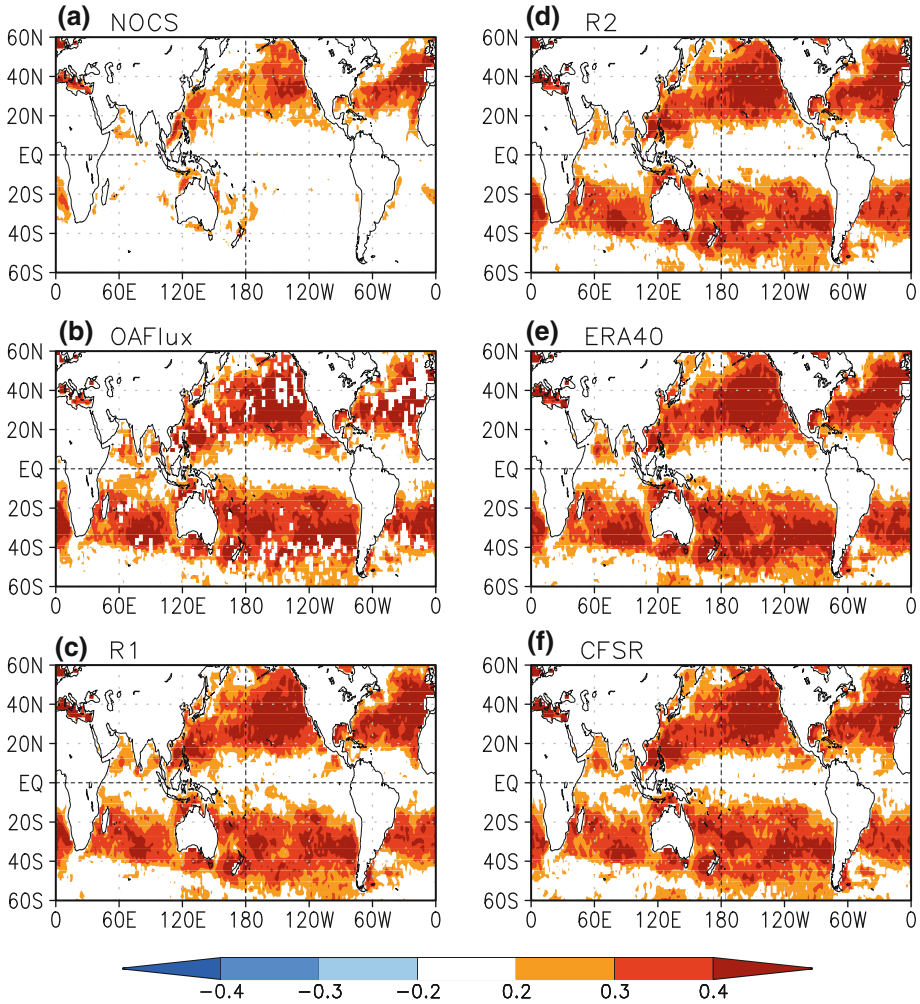

Fig. 16 Correlation between monthly SST tendency and monthly mean net downward surface heat flux from **a** NOCS, **b** OAflux, **c** R1, **d** R2, **e** ERA40, and **f** CFSR. Values that are significant at 95% level are *shaded* at an interval of 0.1 starting from ±0.2

over the ocean in the CFSR is larger than that in the R1 but smaller than that in the R2. Over land, the CFSR produces much less GM evaporation than both R1 and R2.

Interannual variability is analyzed for precipitation and T2m. The R1 precipitation variability in the tropics is too small, while R2, ERA40 and CFSR all produce stronger variability in most of the tropics than the observations. The CFSR precipitation correlation skill in the mid-latitudes is higher than the R1 and R2 but lower than ERA40. In the tropics, the CFSR shows an better performance than the R1, R2 and ERA40. For T2m, the ERA40 shows the best correlation due to its explicit inclusion of the observation in the post-processing. The CFSR T2m is better than R1 and R2 in both the spatial distribution and GM, reflecting the effects of the upgraded model physics and the use of varying green-house gases and aerosol forcing in the CFSR.

Since the CFSR includes both the atmosphere and ocean, it is interesting to examine its representation of the relationships between atmospheric and oceanic fields. One improvement in the CFSR is that it captured the weak SST-precipitation relationship in the subtropical Pacific in observations while the other three reanalyses produced too strong positive precipitation-SST relationships. The local correlation between surface heat flux and SST tendency in the CFSR is significantly positive in the mid- and high-latitudes, indicating the contribution of heat flux in driving SST variations, and near zero in the tropics, implying the importance of oceanic dynamics in SST variability. The correlation between surface heat flux and SST in the CFSR is similar to that in other reanalyses and OAFlux.

A few problems in the long-term variations are identified in the CFSR. Firstly, dramatic changes are found around 1998–2001 in a number of variables, with a substantial increase in precipitation, precipitable water, cloud amount, and decrease in surface evaporation and downward solar radiation flux. These changes are likely related to the transition from TOVS to ATOVS of the assimilated radiance data in 1998 and the assimilation of QuikSCAT

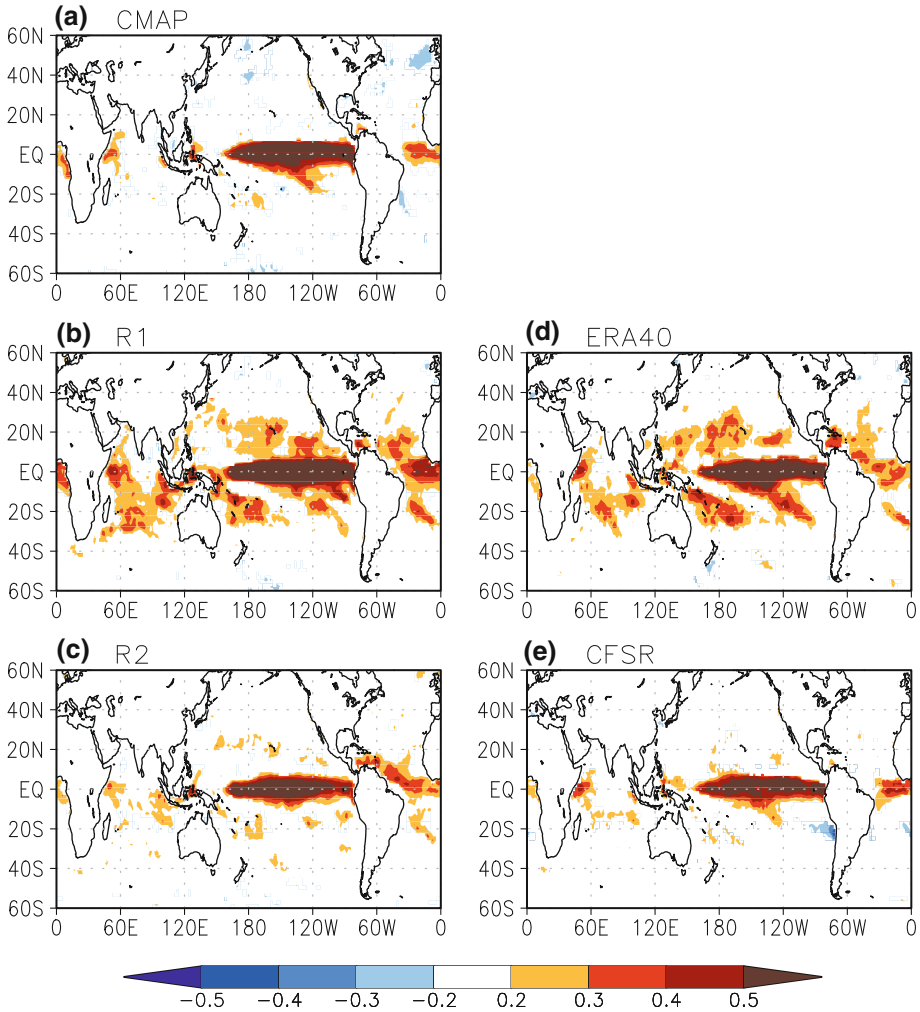

Fig. 17 Correlation between monthly mean SST and precipitation from **a** CMAP, **b** R1, **c** R2, **d** ERA40, and **e** CFSR. Values that are significant at 95% level are *shaded* at an interval of 0.1 starting from ±0.2

surface winds in 2001. Secondly, the use of six streams for the CFSR is found to induce spurious jumps in soil moisture between adjacent streams. In addition, there exist upward or downward soil moisture trends within the streams over various regions, indicating the spin-up time was too short. Thirdly, there is an inconsistency in long-term sea ice extent over the arctic regions between the CFSR and the National Snow and Ice Data Center observation with the CFSR showing smaller sea ice extent before 1997 and larger extent starting in 1997.

Our diagnoses have focused on annual average and global characteristics in the CFSR. Analyses on more detailed features in the CFSR such as the study by Higgins et al. (2010) on precipitation frequency and intensity, and the study by Mo et al. (2010) on local features of drought will help provide a more detailed assessment of the CFSR. In addition, only dynamical fields from the reanalyses have been used in most climate diagnostics, because the convective heating from the previous reanalyses is considered not reliable. The CFSR appears to be more capable of reproducing observed precipitation variability in the Indian Ocean and the western Pacific. It will be interesting to investigate if the CFSR also produces improved diabatic processes and a realistic relationship between the large-scale circulation and convection. Moreover, the problems revealed in this study are based on global or regional averages. Additional studies are required to examine the spatial distribution of the related variables and the relationships among atmospheric and oceanic fields. Further, since the reanalysis largely depends on the model's capability to realistically capture the physical processes over regions of sparse observations, an analysis of the model's deficiencies (for examples, the mean bias and variability errors) without assimilating observations will help understand the causes of the existing problems in the CFSR.

Acknowledgments We thank Robert Grumbine for his helpful comments on the CFSR sea ice analysis. We greatly appreciate the constructive internal reviews by Amy Butler and Boyin Huang. We thank the anonymous reviewer for the valuable comments and suggestions.

References

Adler RF, Huffman GJ, Chang A, Ferraro R, Xie P, Janowiak J, Rudolf B, Schneider U, Curtis S, Bolvin D, Gruber A, Susskind J, Arkin P (2003) The version 2 global precipitation climatology project (GPCP) monthly precipitation analysis (1979-present). J Hydrometeorol 4:1147–1167

Alexander MA, Blade I, Newman M, Lanzante JR, Lau NC, Scott J (2002) The atmospheric bridge: the influence of ENSO teleconnections on air–sea interaction over the global oceans. J Clim 15:2205–2231

Berry DI, Kent EC (2009) A new air–sea interaction gridded dataset from ICOADS with uncertainty estimates. Bull Am Meteorol Soc 90:645–656

Cai M, Shin C, van den Dool HM, Wang W, Saha S, Kumar A (2009) The role of long-term trend in seasonal predictions: implication of global warming in the NCEP CFS. Weather forecast 24:965–973

Chelliah M, Ebisuzaki W, Weaver S, Kumar A (2010) Evaluating the tropospheric analyses from NCEP's climate forecast system reanalysis. Clim Dyn (submitted)

Chou SH, Nelkin E, Ardizzone J, Atlas R, Shie CL (2003) Surface turbulent heat and momentum fluxes over global oceans based on the Goddard satellite retrievals, version 2 (GSSTF2). J Clim 16:3256–3273

Cronin MF, Fairall CW, McPhaden MJ (2006) An assessment of buoy-derived and numerical weather prediction surface heat fluxes in the tropical Pacific. J Geophys Res 111:C06038. doi:10.1029/2005JC003324

Dai A (2006) Precipitation characteristics in eighteen coupled climate models. J Clim 19:4605–4630

Dai A, Karl TR, Sun B, Trenberth KE (2006) Recent trends in cloudiness over the United States: a tale of monitoring inadequacies. Bull Am Meteorol Soc 87:597–606

Ebert EE, Janowiak JE, Kidd C (2007) Near real-time satellite precipitation estimates—accuracy and comparison with numerical model outputs. Bull Am Meteorol Soc 88:47–64

Fan Y, van den Dool H (2008) A global monthly land surface air temperature analysis for 1948-present. J Geophys Res 113: D01103. doi:10.1029/2007JD008470

Francis JA, Chan W, Leathers DJ, Miller JR, Veron DE (2009) Winter Northern Hemisphere weather patterns remember summer Arctic sea-ice extent. Geophys Res Lett 36:L07503. doi:10.1029/2009GL037274

Gibson JK, Kallberg P, Uppala S, Nomura A, Hernandez A, Serrano E (1997) ERA description. In: ECMWF ERA-15 Project Report Series, No. 1. European Centre for Medium-Range Weather Forecasts, Shinfield, Reading, UK. http://www.ecmwf.int/publications

Grassl H, Jost V, Schulz J, Ramesh Kumar MR, Bauer P, Schluessel P (2000) The Hamburg ocean–atmosphere parameter and fluxes from satellite data (HOAPS): a climatological Atlas of satellite-derived air–sea interaction parameters over the World Oceans. Report No. 312, ISSN 0937-1060, Max Planck Institute for meteorology, Hamburg, p 130 + figures

Grumbine RW (2009) A posteriori filtering of sea ice concentration analyses. MMAB Tech. Note 282, NCEP, p 7

Grumbine RW (2010a) Operational NCEP sea ice concentration analysis (in preparation)

Grumbine RW (2010b) CFSR sea ice analysis (in preparation)

Higgins RW, Kousky VE, Silva VBS, Becker E, Xie P (2010) Intercomparison of daily precipitation statistics over the United States in observations and in NCEP reanalysis products. J Clim 23:4637–4650

Huang B, Mehta VM, Schneider N (2005) Oceanic response to idealized net atmospheric freshwater in the Pacific at the decadal timescale. J Phys Oceanogr 35:2467–2486

Josey SA, Kent EC, Taylor PK (1998) The Southampton Oceanography Centre (SOC) ocean–atmosphere heat, momentum and freshwater flux Atlas. Southampton Oceanography Centre Rep. 6, p 30 + figures

Josey SA, Kent EC, Taylor PK (1999) New insights into the ocean heat budget closure problem from analysis of the SOC air–sea flux climatology. J Clim 12:2850–2880

Joyce RJ, Janowiak JE, Arkin PA, Xie P (2004) CMORPH: a method that produces global precipitation estimates from passive microwave and infrared data at high spatial and temporal resolution. J Hydrometeorol 5:487–503

Kalnay E et al (1996) The NCEP/NCAR 40-year reanalysis project. Bull Am Meteorol Soc 77:437–471

Kanamitsu M, Ebisuzaki W, Woolen J, Yang SK, Hnilo J, Fiorino M, Potter GL (2002) NCEP–DOE AMIP-II reanalysis (R-2). Bull Am Meteorol Soc 83:1631–1643

Kistler R et al (2001) The NCEP–NCAR 50-year reanalysis: monthly means CD-ROM and documentation. Bull Am Meteorol Soc 82:247–268

Krishna Kumar K, Hoerling M, Rajagopalan B (2005) Advancing dynamical prediction of Indian monsoon rainfall. Geophys Res Lett 32:L08704. doi:10.1029/2004GL021979

Kumar A, Hoerling MP (1998) On the specification of regional SSTs in AGCM simulations. J Geophys Res 103:8901–8907

Long CS, Butler AH, Lin R, Wild J, Yang SK, Zhou S, Liu H (2010) Evaluation of the stratosphere in the NCEP climate forecast system reanalysis. Clim Dyn (submitted)

Mo K, Long LN, Xia Y, Yang SK, Schemm JE, Ek M (2010) Drought indices based on the climate forecast system reanalysis and ensemble NLDAS. J Hydrometeorol (submitted)

Moore GWK, Renfrew IA (2002) An assessment of the surface turbulent heat fluxes from the NCEP–NCAR reanalysis over the western boundary currents. J Clim 15:2020–2037

Onogi K, Tsutsui J, Koide H, Sakamoto M, Kobayashi S, Hatsushika H, Matsumoto T, Yamazaki N, Kamahori H, Takahashi K, Kadokura S, Wada K, Kato K, Oyama R, Ose T, Mannoji N, Taira R (2007) The JRA-25 reanalysis. J Meteorol Soc Japan 85:369–432

Reynolds RW, Smith TM, Liu C, Chelton DB, Casey KS, Schlax MG (2007) Daily high-resolution blended analyses for sea surface temperature. J Clim 20:5473–5496

Roads J (2003) The NCEP–NCAR, NCEP–DOE, and TRMM tropical atmosphere hydrologic cycles. J Hydrometeorol 4:826–840

Saha S et al (2010) The NCEP climate forecast system reanalysis. Bull Am Meteorol Soc 91:1015–1057

Schubert S, Park CK, Wu CY, Higgins W, Kondratyeva Y, Molod A, Takacs L, Seablom M, Rood R (1995) A multi-year assimilation with the GEOS-1 system: overview and results'. NASA Tech. Rep. series on global modeling and data assimilation, No. 6. In: Suarez MJ (ed) NASA, Goddard Flight Center, Greenbelt

Serreze MC, Barrett AP, Stroeve JC, Kindig DN, Holland MM (2009) The emergence of surface-based Arctic amplification. Cryosphere 3:11–19

Shinoda T, Alexander MA, Nehdon HH (2004) Remote response of the Indian Ocean to interannual SST variations in the tropical Pacific. J Clim 17:362–372

Simpson JR, Adler RF, North GR (1988) A proposed tropical rainfall measuring mission (TRMM) satellite. Bull Am Meteorol Soc 69:278–295

Smith SR, Legler DM, Verzone KV (2001) Quantifying uncertainties in NCEP reanalyses using high-quality research vessel observations. J Clim 14:4062–4072

Tomita H, Kubota M, Cronin MF, Iwasaki S, Konda M, Ichikawa H (2010) An assessment of surface heat fluxes from J-OFURO2 at the KEO/JKEO sites. J Geophys Res 115. doi:10.1029/2009JC005545

Trenberth KE, Smith L, Qian T, Dai A, Fasullo J (2007) Estimates of the global water budget and its annual cycle using observational and model data. J Hydrometeorol 8:758–769

Trenberth KE, Fasullo JT, Kiehl J (2009) Earth's global energy budget. Bull Am Meteorol Soc 90:311–323

Uppala SM et al (2005) The ERA-40 re-analysis. Q J R Meteorol Soc 131:2961–3012

Wang B, Wu R, Li T (2003) Atmosphere–warm ocean interaction and its impacts on Asian–Australian monsoon variation. J Clim 16:1121–1195

Wang W, Chen M, Kumar A (2010) An assessment of the CFS real-time forecast. Weather Forecast 25:950–969

Wu R, Kirtman BP (2005) Roles of Indian and Pacific Ocean air–sea coupling in tropical atmospheric variability. Clim Dyn 25:155–170

Wu R, Kinter JL III, Kirtman BP (2005) Discrepancy of interdecadal changes in the Asian region among the NCEP–NCAR reanalysis, objective analyses, and observations. J Clim 18:3048–3067

Xie P, Arkin PA (1997) Global precipitation: a 17-year monthly analysis based on gauge observations, satellite estimates and numerical model outputs. Bull Am Meteorol Soc 78:2539–2558

Xie P, Chen M, Shi W (2010) CPC unified gauge analysis of global daily precipitation. J Hydrometeorol (to be submitted)

Xue Y, Huang B, Hu ZZ, Kumar A, Wen C, Behringer D (2010) An assessment of oceanic variability in the NCEP climate forecast system reanalysis. Clim Dyn (submitted)

Yu L, Weller RA (2007) Objectively analyzed air–sea heat fluxes for the global ice-free oceans (1981–2005). Bull Am Meteorol Soc 88:527–539

Yu L, Jin X, Weller RA (2006) Role of net surface heat flux in seasonal variations of sea surface temperature in the tropical Atlantic Ocean. J Clim 19:6153–6169

Yu L, Jin X, Weller RA (2007) Annual, seasonal, and interannual variability of air–sea heat fluxes in the Indian Ocean. J Clim 20:3190–3209

Yu L, Jin X, Weller RA (2008) Multidecade global flux datasets from the objectively analyzed air–sea fluxes (OAFlux) project: latent and sensible heat fluxes, ocean evaporation, and related surface meteorological variables. Woods Hole Oceanographic Institution, OAFlux Project Technical Report. OA-2008-01, Woods Hole, p 64

Zhang Y, Rossow W, Lacis A, Oinas V, Mishchenko M (2004) Calculation of radiative flux profiles from the surface to top-of atmosphere based on ISCCP and other global data sets: refinements of the radiative transfer model and input data. J Geophys Res 109. doi:10.1029/2003JD004457